Electronic Supplementary Material (ESI) for Dalton Transactions.

MnO_2 Nanoflower Grown on a Polypropylene Separator as Both Barrier and Accelerator of polysulfides for High-performance Li–S Batteries

*Yinze Zuo[a,b], Tao Yan[a,b], Yuejin Zhu[a,d], Jian Zhou[a,b], Weiming Su[a,b**], Xingling Shi[e], Yuefeng Tang[a,b,c*] and Yanfeng Chen[a,b]*

[a]National Laboratory of Solid State Microstructures, Jiangsu Key Laboratory of Artificial Functional Materials, College of Engineering and Applied Sciences, Nanjing University, Nanjing, China.
[b]Collaborative Innovation Center of Advanced Microstructures, Nanjing University, Nanjing, China.
[c]SuZhou Sun Sources Nano Science and Technology Co. Ltd., ChangShu, SuZhou 215513, China.
[d]Institute of Advanced Synthesis, School of Chemistry and Molecular Engineering, Nanjing Tech University, Nanjing, China.
[e]School of Materials Science and Engineering, Jiangsu University of Science and Technology, Zhenjiang, China.
E-mail: *yftang@nju.edu.cn, **jimgrange@sina.com.

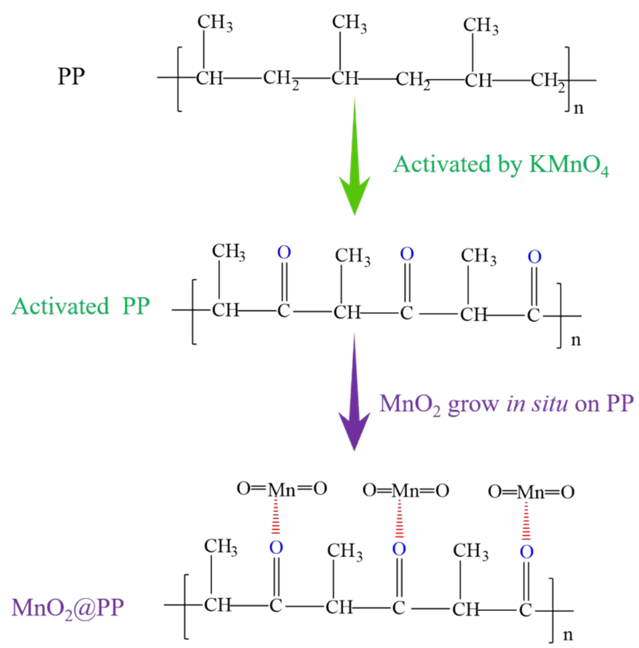

Figure S1. Schematic illustration of growth mechanism for the MnO_2@PP separator.

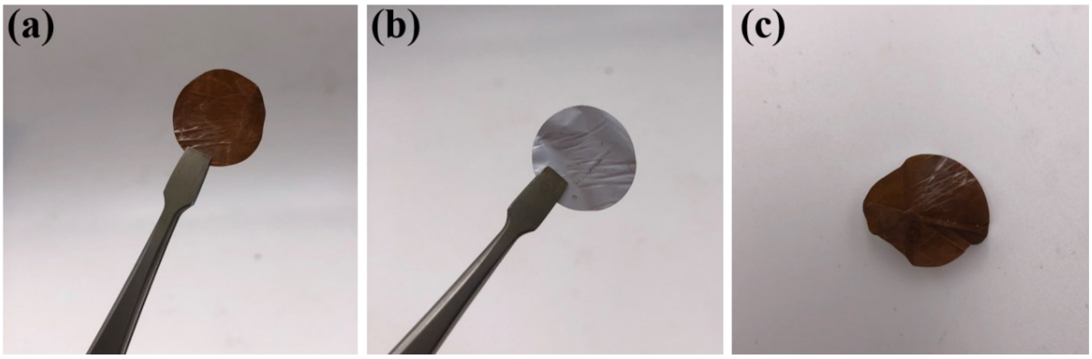

Figure S2. The digital photograph of the front side and reverse side of MnO_2@PP separator and the kneading/spreading test of the MnO_2@PP separator.

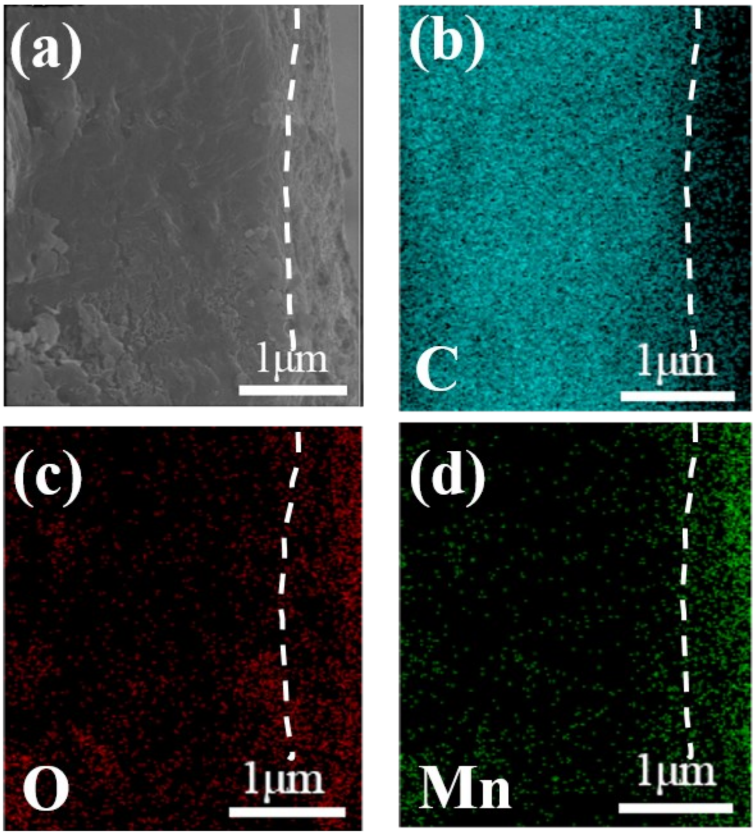

Figure S3. (a) Cross-sectional morphologies of MnO_2@PP separator, and corresponding elemental mapping images of (b) C, (c) O, (d) Mn.

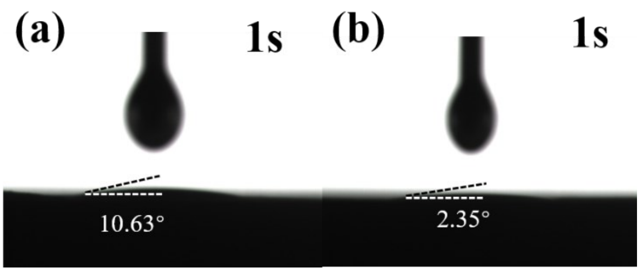

Figure S4. Contact angle measurements of (a) pristine separator; and (b) MnO_2/PP separator for the electrolyte.

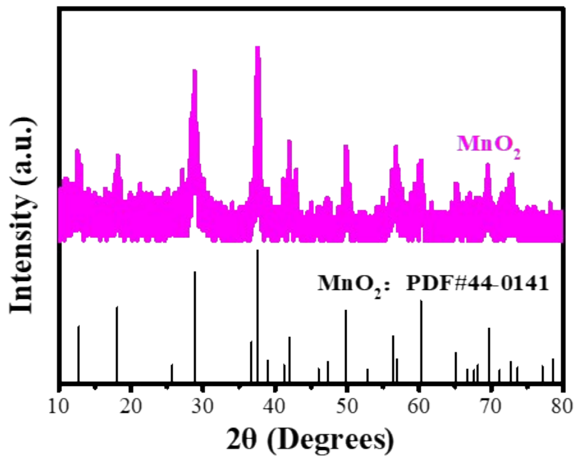

Figure S5. The XRD pattern of the MnO_2 powders stripped from the MnO_2@PP separator.

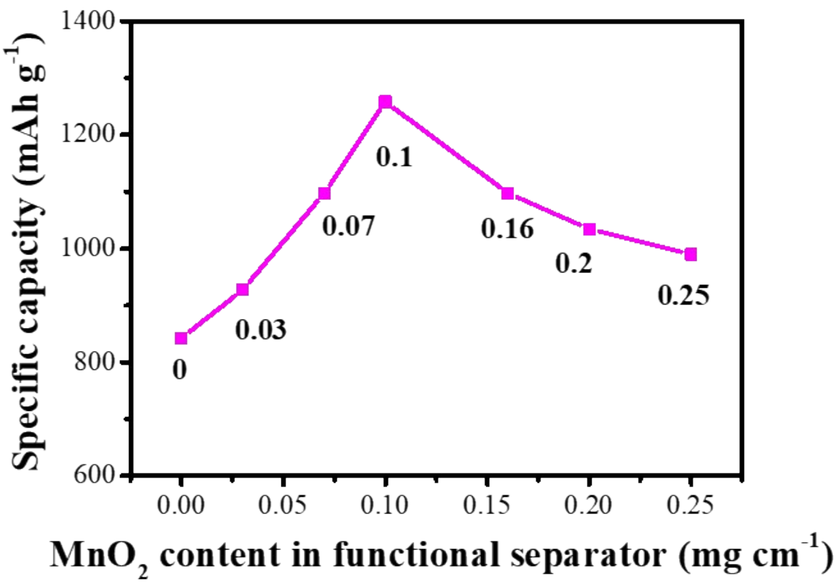

Figure S6. Capacity optimization of MnO_2 content in the MnO_2@PP separator.

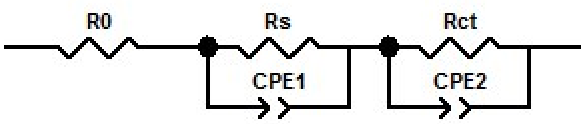

Figure S7. The equivalent circuit diagram of the Nyquist plots.

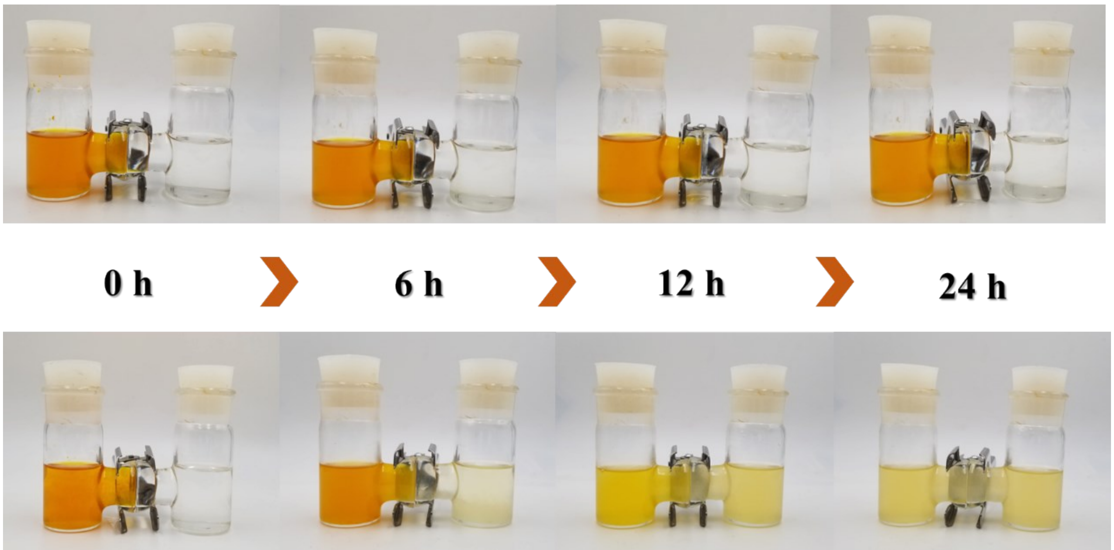

Figure S8. Digital photographs of the Li_2S_6 diffusion tests for the MnO_2@PP separator (top) and PP separator (bottom)

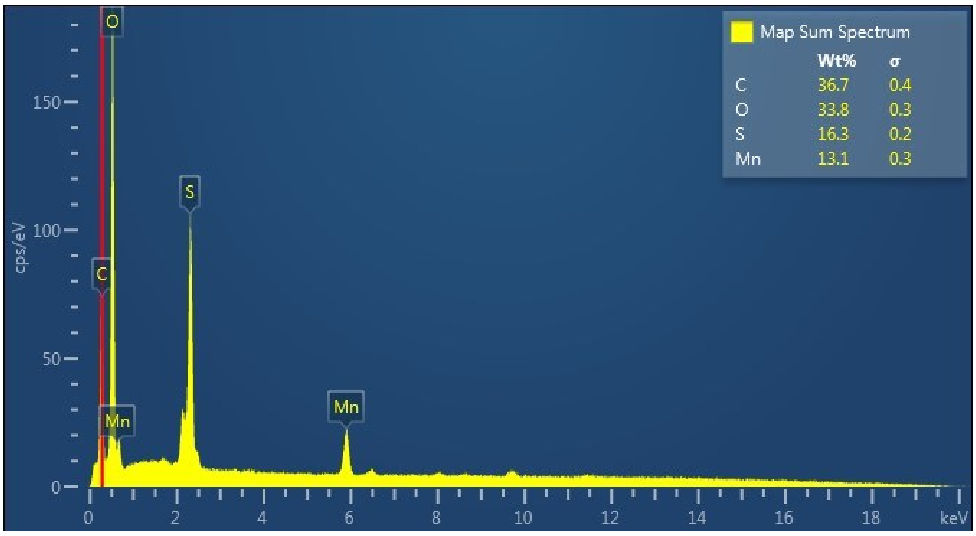

Figure S9. EDX spectra of MnO_2@PP separator after cycling.

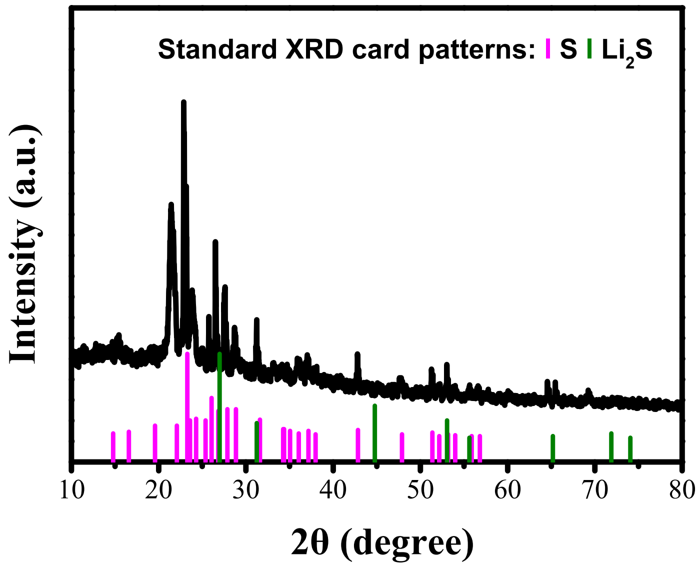

Figure S10. XRD patterns of MnO_2@PP separator after cycling and standard XRD patterns sulfur and Li_2S powder.

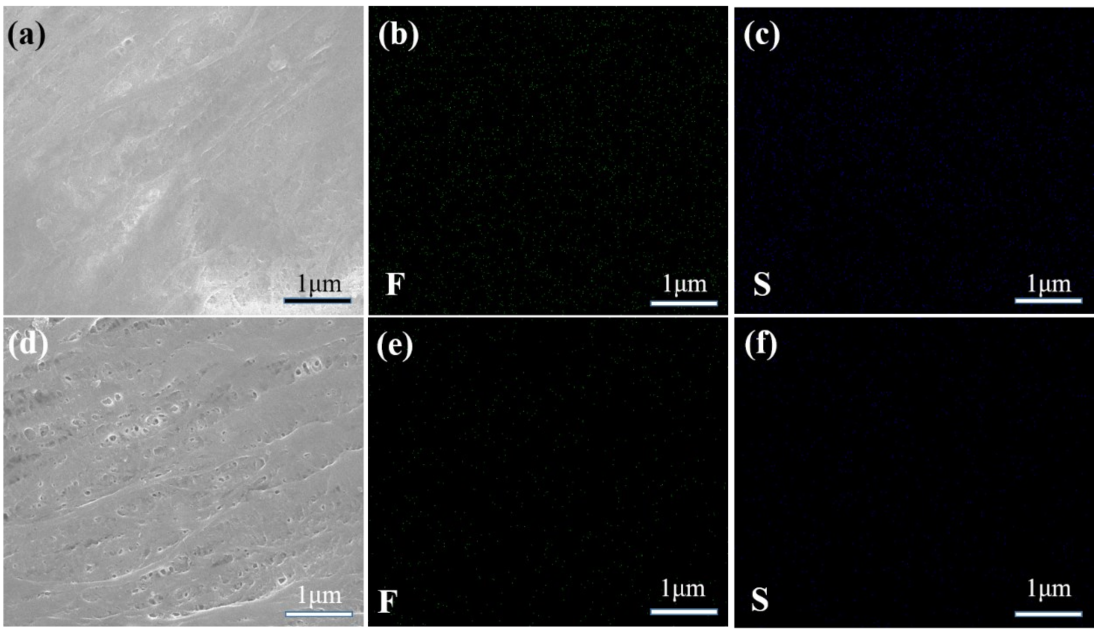

Figure S11. The SEM images and corresponding elemental mapping images of (a,b,c)PP and (d,e,f)MnO_2@PP separator after cycling.

Table S1. Comparison of electrochemical properties functional separators in Li–S cells.

Coating or interlayer	Thickness	Sulfur loading	Sulfur content	Cathode	Discharge Capacity	Areal capacity (mAh	E/S ratio	Ref

						cm^{-2})		
MoO_3@CNT	N/A	1.0	60%	Super P/S	~755 mAh g^{-1}, 200th, 0.3 C	<2.0	N/A	S1
EUC-CNF	N/A	1.5	70%	Super P/S	1038 mAh g^{-1}, 50th, 0.2 C	<2.0	N/A	S2
SSNS/CNT	10μm	1.0	65%	KB/S	680 mAh g^{-1}, 100th, 0.2 C	<2.0	N/A	S3
GO@MoS_2	8μm	3.64	70%	CB/S	~600 mAh g^{-1}, 95th, 0.2 C	2.2	14	S4
TiO_2/C	80μm	1.1	54%	AB/S	1000 mAh g^{-1}, 60th, 0.1 C	<2.0	36	S5
CNF@ZrO_2	N/A	2.7	70%	CB/S	800 mAh g^{-1}, 60th, 0.2 C	~2.1	40	S6
rGO@SL	0.8nm	3.8	75%	CB/S	700 mAh g^{-1} 50th, 0.05 C	2.7	8	S7
TiN	25μm	1.3	70%	Super P/S	744 mAh g^{-1} 200th, 0.5 C	<2.0	46	S8
MnO_2	380nm	1.5-2.5	66%	KB/S	~603 mAh g^{-1}, 500th, 0.5 C	<2.0	8.8	S9
MnO_2@PP	500nm	6	70%	CB/S	~747 mAh g^{-1}, 150th, 0.2 C	~6	~6.6	This work

References

[S1] L. Y. Luo, X. Y. Qin, J. X. Wu, G. M. Liang, Q. Li, M. Liu, F. Y. Kang, G. H. Chen, B. H. Li, An interwoven MoO_3@CNT scaffold interlayer for high-performance lithium–sulfur batteries, *J. Mater. Chem. A*, 2018, **6**, 8612-8619.

[S2] K. S. Wu, Y. Hu, Z. Shen, R. Z. Chen, X. He, Z. L. Cheng and P. Pan, Highly efficient and green fabrication of a modified C nanofiber interlayer for high-performance Li-S batteries, *J. Mater. Chem. A,* 2018, **6**, 2693-2699.

[S3] S. S. Yao, J. C, J. Q. Huang, Z. H. Lu, Y. Deng, W. G. Chong, J. X. Wu, M. Haq, F. Ciucci and J. K. Kim, Novel 2D Sb_2S_3 nanosheet/CNT coupling layer for exceptional polysulfide recycling performance, *Adv. Energy Mater.,* 2018, 1800710.

[S4] L. Tan, X. H. Li, Z. X. Wang, H. J. Guo, J. X. Wang, Lightweight reduced graphene oxide@MoS_2 interlayer as polysulfide barrier for high-performance lithium-sulfur batteries, ACS Appl. Mater. Interfaces, 2018, **10**, 3707-3713.

[S5] S. Y. Liu, C. Y. Fan, Y. H. Shi, H. C. Wang, X. L. Wu, J. P. Zhang, Effective cathode design of three-layered configuration for high-energy Li–S batteries, ACS Appl. Mater. Interfaces, 2018, **10**, 509-516.

[S6] Y. Li, J. Zhu, R. Shi, M. Dirican, P. Zhu, C. Yan, H. Jia, J. Zang, J. He, X. Zhang, Ultrafine and polar ZrO_2-inlaid porous nitrogen-doped carbon nanofiber as efficient polysulfide absorbent for high-performance lithium-sulfur batteries with long lifespan, *Chem. Eng. J.,* 2018, **349**, 376-387.

[S7] Z. Z. Du, C. K. Guo, L. J. Wang, A. J. Hu, S. Jin, T. M. Zhang, H.C. Jin, Z. K. Qi, S. Xin, X. H. Kong, Y. G. Guo, H. X. Ji, L. J. Wan, Atom-Thick Interlayer Made of CVD-Grown Graphene Film on Separator for Advanced Lithium−Sulfur Batteries, A*CS Appl. Mater. Interfaces*, 2017, **9**, 43696–43703.
[S8] B. Y. Hao, H. Li, W. Lv, Y. B. Zhang, S. Z. Niu, Q. Qi, S. J. Xiao, J. Li, F. Y. Kang, Q. H. Yang, Reviving catalytic activity of nitrides by the doping of the inert surface layer to promote polysulfide conversion in lithium-sulfur batteries, *Nano Energy*, 2019, **60**, 305-311.
[S9] X. Song, G. P. Chen, S. Q. Wang, Y. P. Huang, Z. Y. Jiang, L. X. Ding, H. H. Wang, Self-Assembled Close-Packed MnO_2 Nanoparticles Anchored on a Polyethylene Separator for Lithium−Sulfur Batteries, *ACS Appl. Mater. Interfaces,* 2018, **10**, 26274-26282.